Atmospheric Research 299 (2024) 107223

Contents lists available at ScienceDirect

Atmospheric Research

journal homepage: www.elsevier.com/locate/atmosres

Numerical investigation of the Pedrógão Grande pyrocumulonimbus using a fire to atmosphere coupled model

Flavio Tiago Couto [a,*], Jean-Baptiste Filippi [b], Roberta Baggio [b], Cátia Campos [c], Rui Salgado [a]

[a] Instituto de Ciências da Terra – ICT (Polo de Évora), Instituto de Investigação e Formação Avançada – IIFA, Earth Remote Sensing Laboratory (EaRS Lab), Departamento de Física, Escola de Ciências e Tecnologia, Universidade de Évora, Rua Romão Ramalho, 59, 7000-671 Évora, Portugal
[b] Centre National de la Recherche Scientifique (CNRS), Sciences Pour l'Environnement – Unité Mixte de Recherche 6134, Università di Corsica, Campus Grossetti, Corte, France
[c] Instituto de Ciências da Terra – ICT (Polo de Évora), Earth Remote Sensing Laboratory (EaRS Lab), Universidade de Évora, Rua Romão Ramalho, 59, 7000-671 Évora, Portugal

ARTICLE INFO

Keywords:
pyroCb
Mega fires
Meso-NH model
ForeFire model
Pedrógão Grande fire

ABSTRACT

Understanding the development of fire-generated thunderstorms in mega fire events is important given their high impact on the evolution of the fire fronts, where the fire spread becomes highly unpredictable and difficult to suppress. This study aims to investigate numerically the influence of strong pyro-convective activity on the local atmospheric conditions by means of a numerical simulation based on the coupled Meso-NH/ForeFire code. To our knowledge, it is the first time that the effect of wildfire spread on the local atmospheric conditions is accounted explicitly in a high-resolution NWP model to investigate pyro-convection activity. More specifically, we study numerically the Portuguese Pedrógão Grande mega fire, which was one of the most destructive and deadliest wildfire hazards affecting the Mediterranean region in the recent years. The spatio-temporal propagation of the wildfire was assigned a priori on the basis of the official investigation's reports, while the impact of the forced fire evolution and of the ensuing heat and water vapour emissions on the local atmospheric conditions is accounted explicitly. The simulation, configured with very-high spatial and temporal resolutions, was capable of resolving the intense convective column reaching the upper troposphere and the fast development of the associated cloud system. The numerical fire produced intense updraughts with vertical velocities above 15 m/s, whereas the associated pyroCb cloud was composed by five different hydrometeor species along the main convective column and reached an altitude of 10 km. It is remarkable that the numerical experiment reproduced phenomena occurring at a fine scale related to cloud microphysics, such as very-localized outflows. This study, based on a coupled numerical simulation, was capable of illustrating in detail the development of a pyroCb cloud from strong pyro-convective activity.

1. Introduction

Extreme wildfires are frequently associated with strong convective processes due to the release of heat and moisture. However, the evolution of the local atmospheric conditions surrounding the fire is not fully understood, and some associated phenomena (strong gusts, fire acceleration, wind shifts) are still poorly quantified.

The local atmospheric environment surrounding the fire may present the formation of convective clouds, also referred as pyroCumulus (pyroCu) or pyroCumulonimbus (pyroCb). PyroCu is more common and forms as a cloud within a fire's plume, and is a necessary precursor to pyroCb. PyroCb can be observed in plume dominated wildfires characterized by an intense convective column, above which a cumulonimbus (Cb) cloud develops. The formation of a pyroCb cloud requires a core of buoyant plume rising to the level of free convection in an atmospheric environment that enables deep, moist convection (Tory et al., 2018). However, the presence of burning biomass and aerosols in the upper troposphere influences the microphysics of such clouds, which includes pyrometeors (e.g., McCarthy et al., 2019). Moreover, the fire-generated cloud system can induce the ignition of new fires by lightning activity (e.g., Lang et al., 2014) and condensation of moisture in the smoke plume can enhance convection by releasing latent heat with updraughts

* Corresponding author.
E-mail addresses: fcouto@uevora.pt (F.T. Couto), filippi_j@univ-corse.fr (J.-B. Filippi), baggio_r@univ-corse.fr (R. Baggio), catia.campos@uevora.pt (C. Campos), rsal@uevora.pt (R. Salgado).

https://doi.org/10.1016/j.atmosres.2024.107223
Received 10 July 2023; Received in revised form 27 October 2023; Accepted 1 January 2024
Available online 3 January 2024

penetrating the stratosphere (e.g., Fromm and Servranckx, 2003; Fromm et al., 2010; Tarshish and Romps, 2022).

For instance, Peterson et al. (2018) showed that in August 2017 the mass of smoke aerosol particles injected into the lower stratosphere from five near-simultaneous pyroCb was comparable to a moderate volcanic eruption. Fromm et al. (2021) studied the same time period and revealed at least two pyroCb clouds injecting smoke above 13.5 km up to 2.5 km above the local tropopause. Over Canada, the extreme pyroCb activity recorded in August 2017 also resulted in a high-arctic smoke event (Ranjbar et al., 2019). Gerasimov et al. (2019) revised the results of lidar measurements of stratospheric aerosol over Tomsk (Russia) and discovered traces of aerosol from pyroCb events that occurred in North America a few weeks before. The presence of smoke in the lower stratosphere over Tomsk was also recently identified by Cheremisin et al. (2022) as a consequence of the Siberian wildfires in August 2019. In the Southern hemisphere, in turn, a pyroCb outbreak in Australia during the 2019/2020 summer injected large smoke particle amounts into the lower stratosphere (e.g., Khaykin et al., 2020; Peterson et al., 2021).

In general, pyroCb studies are based on remote sensing, which can quantify and analyze these intense smoke events. However, some of the pyroCb-related phenomena, crucial for the firefighter's safety as it may drastically change the fire behavior, requires very high temporal and spatial resolution to be fully resolved. For instance, McRae et al. (2015) documented atypical local fire dynamics, in particular the fire channeling phenomenon, also known as Vorticity-driven Lateral Spread (VLS) (Sharples and Hilton, 2020), which resulted in a rapid, but also sudden, spread of the fire front due to an interaction between fire, local terrain, and atmospheric conditions.

Lareau et al. (2018) described a sequence of events leading to vortex development at a pyroCb scale. The authors showed that a tornado-strength vortex formed as a consequence of the pre-existing shear zone during the rapid vertical development of the pyro cloud system. According to Lareau et al. (2022), this phenomenon is potentially deadly and poorly understood.

The study of pyroCb is made even more important by the fact that climate change is likely to increase the number and the severity of wildfires associated with extreme pyroCb's outbreaks (e.g., Dowdy et al., 2019). Recently, Senande-Rivera et al. (2022) showed that the number of days with high fire risk will increase significantly across southern Europe, especially in the Iberian Peninsula and Southern France. In 2017, there were significant mega fires (i.e., a fire with a burned area above 10,000 ha, Linley et al. (2022)) across mainland Portugal causing more than one hundred fatalities in June and October (e.g., CTI Report, 2017; Guerreiro et al., 2018). Although the 2022 fire season only recorded one mega fire in Portugal, Couto et al. (2022) showed that in the last decade the actual number of active fires has grown in the country. In particular, they reported a large fire event occurring during the winter season, thus supporting the thesis that climate change is likely to enhance occurrence of large fires out of the expected season.

The use of coupled fire-atmosphere simulations may provide a valid support to an improved understanding of the complexities associated with fire-atmosphere interaction. We address some of the major problems linked to mega fires, by studying in detail the influence of an extreme wildfire on the atmosphere using a fire to atmosphere simulation. In this work we investigate the pyro-convective activity by using a numerical experiment, performed with the Meso-NH non-hydrostatic atmospheric model coupled to the ForeFire fire propagation model. This coupled code has been successfully used in the last years (e.g., Filippi et al., 2018; Baggio et al., 2022; Campos et al., 2023), however, this is the largest real case in which this coupled code has been applied. With respect to cloud resolving models (e.g., Trentmann et al., 2006; Luderer et al., 2006; Cunningham and Reeder, 2009; Badlan et al., 2021a, 2021b), this coupled approach allows us to account explicitly for the fire-to-atmosphere interactions.

The paper is organized as follows: the next section describes the methodology, whereas Section 3 contains the results that are discussed in Section 4. The conclusions of the study are presented in Section 5.

2. Methodology

The Meso-NH is a full-physics non-hydrostatic limited-area research model able to represent the atmospheric motions at different scales (Lac et al., 2018). In this study, we exploited the Meso-NH grid-nesting capability to progressively increase the horizontal resolution, by dividing the simulated areas in nested domains, such that the finest grid covers the region of the spreading fire. In this way, it was possible to solve both close range fire to atmosphere interactions and large-scale atmospheric effects while keeping reasonable computational costs.

The atmospheric model runs with a parameterization package of sub-grid scale physical processes. The radiation parameterization is based on the Rapid Radiative Transfer Model (Mlawer et al., 1997), whereas the turbulence scheme is based on a 1.5-order closure (Cuxart et al., 2000). In the inner domains, the full 3D turbulent fluxes scheme was activated (Verrelle et al., 2015), while in the coarser domain only the vertical fluxes were considered. Cloud microphysics is modelled by the ICE3 one-moment bulk microphysical parameterization scheme (Pinty and Jabouille, 1998). The scheme considers six categories of hydrometeors and a prognostic equation for each one. Besides vapour, it predicts the mixing ratio of other five water categories: cloud droplets, rain drops, pristine ice crystals, snow-aggregates and graupel. The parameterization of several microphysical processes allows the computation of the multiple complex interactions between the different hydrometeor types. Despite the fact that the micro and nanoparticles emitted by the fire significantly affect precipitation, in the simulations discussed below the physics of aerosols is not accounted for. The observed fire induced precipitation results from the heat and vapour injection reacting with the water species present in the atmosphere. Since the spatial resolutions considered in this study, deep and shallow convection are explicitly resolved by the model.

Except for the evolving fire front, which is accounted by ForeFire, the other processes involving surface-atmosphere interactions are computed by the externalised platform of surface models, SURFEX (Masson et al., 2013). The topography is obtained from the Shuttle Radar Topography Mission (SRTM) database, whereas the surface has been characterized from the ECOCLIMAP database and the Harmonized World Soil Database (HWSD) soil databases (sand and clay) (Champeaux et al., 2005).

ForeFire is a fire propagation model that can be coupled to the Meso-NH such that the effects of the temporal evolution of the fire front and the ensuing energy and vapour fluxes are explicitly considered in the atmospheric computations. The model considers the terrain slope, the atmospheric properties, the spatial distribution and the combustion parameters of the fuel. The fire propagation is assumed to occur perpendicularly to the fire front (Filippi et al., 2009, 2011).

To evaluate the energy released by the fire, we consider that the study region consists of large areas of mixed coniferous forest, the fuel was assumed to be homogeneous following fuel model 11 from Anderson (1982) with an average of burning fuel load of 2.5 $Kg.m^{-2}$ at 30% humidity (0.75 Kg of water, 1.75 kg of combustible per square meter). Combustion enthalpy is taken at $Dh = 1.5 \times 10^7$ J/kg and evaporation $Dhw = 2.3 \times 10^6$ J/kg, which results in a total energy released after drying of 2.4525×10^7 J/m^2, but only 40% of this energy is assumed to be effective fluxes heating the atmosphere, as combustion can be incomplete and most of the energy is lost in radiation toward the ground and to heat the combustible up to pyrolysis temperature. In the model configuration, the resulting 0.75 kg/m^2 of water vapour and 10×10^6 J/m^2 are released in the atmosphere at the location of the moving fire front for a 1000s "burn duration", resulting in instantaneous fluxes of 0.75 $g.m^{-2}.s$ of water vapour and 10 $KW.m^{-2}$. In the model, fluxes are prescribed at the resolution of the fire within the zone between the fire front at a given time T and the fire front at T − burn duration. This leads to substantial flame depth in areas where the front velocity is at its

maximum.

The treatment of heat fluxes in the ForeFire model can be found in Filippi et al. (2009, 2018). The smoke plume will be illustrated using the relative smoke tracer concentration variable (S). The description of the S variable can be found in Baggio et al. (2022).

The MesoNH/foreFire code can be used in multiple settings. It is possible to simulate the double feedback between the fire propagation and the local atmospheric conditions, that is, the fire enhances the convective motions near the front which in turn affect its spreading of the fire (two-way coupling). Another possible setting is to directly impose the evolution of the fire front with a pre-defined time of arrival map (one-way coupling) and consider the effects on the atmospheric conditions resulting from it. Indeed, a highly detailed fire evolution map, based on the reports of the Portuguese authorities, is directly available. In Fig. 1 we show the fire front at 2000 UTC, on 17th June, in the two simulations (forced fire from observation and fully coupled). While the fully coupled simulation yields similar pyroCb formations and fireline shape when compared to observations, it cannot surpass the accuracy of direct, highly detailed observations, which we use to minimize uncertainty in fire behavior. Considering that in this work we are mostly interested in the fire to atmosphere phenomena, we focus on the latter approach.

The study considers the fires occurred in "Pedrógão Grande" (28,914 ha) and "Góis" (17,521 ha), both started on 17th June 2017. According to Couto et al. (2020), the fires ignited under a dry thunderstorm environment, marked by exceptionally hot and dry air at lower levels and a more humid layer in the middle levels. The fire propagation map is based on the maps presented in the official report of the Portuguese authorities (CTI Report, 2017) and by Pinto et al. (2022). It is noteworthy that "Pedrógão Grande" fire started as a consequence of ignitions in "Regadas" and "Escalos Fundeiros" and was the deadliest event occurred in 2017, with >60 fatalities (e.g., CTI Report, 2017).

The experiment was designed with three two-way nested domains with 300 × 300 grid points (Fig. 2). The outer domain with a coarser grid spacing of 2 km was designed to resolve the mesoscale environment, which measures 600 × 600 km. The resolution is increased by a factor of 5 with an intermediary domain of 400 m resolution and an innermost domain of 80 m resolution. The latter was configured to explore the atmospheric features of the fire-scale environment in detail. The 80 m resolution domain is the one that is actually coupled with the fire and contains the entire burning area. Previous study with the same coupled code (Baggio et al., 2022) shows that 80-m resolution is adequate to solve convective effects on the atmosphere for fires with sufficient energy release, in particular plume rise, cloud formation and downbursts. The vertical grid was configured with 50 sigma levels not equally spaced, stretching gradually from 30 m, near the bottom, to 900 m, near the top. A 30 m first layer height serves as a reasonable tradeoff for capturing fire behavior while minimizing computational load on the pressure solver, especially given the atmospheric model's limitations in handling combustion (extreme heat) and the complex orography of the region. Initial and lateral boundary conditions for the outer domain were provided by ECMWF analysis, with updates every 6 h. The Sea Surface Temperature field was taken from the starting ECMWF analysis and kept constant throughout the simulation.

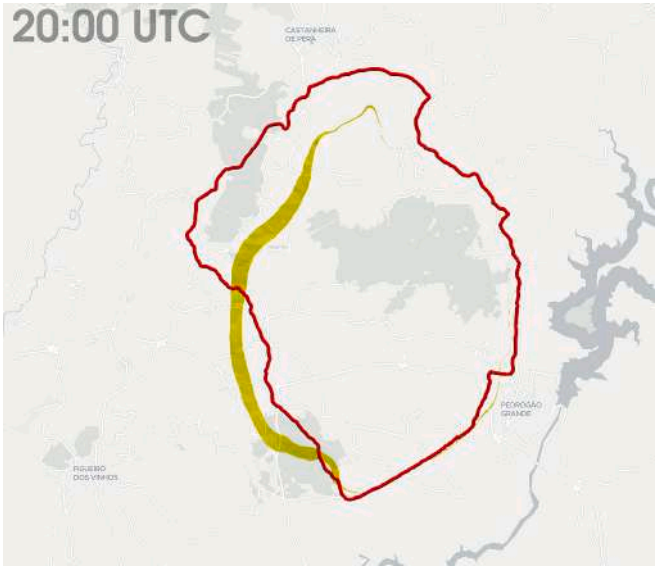

Fig. 1. Fire front line from the fully coupled simulation (red line) and from the forced fire simulation obtained from observation (yellow line) at 2000 UTC on 17th June 2017. (For interpretation of the references to colour in this figure legend, the reader is referred to the web version of this article.)

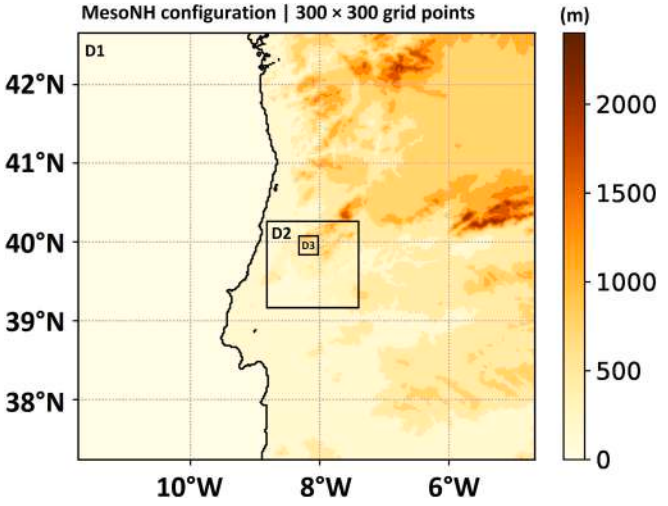

Fig. 2. Model configuration with larger domain at 2 km horizontal resolution (D1) and the inner domains at 400 m (D2) and 80 m (D3) horizontal resolutions. The orography (coloured areas) is obtained from the SRTM database.

In order to study the dynamics of the phenomenon, the frequency for diagnostic output files was set at 10s (80 m resolution), 100 s for the 400 m and 600 s for the larger model. Simulation of the fire model (heat fluxes computation) is performed on a 20 m resolution grid (1200 by 1200). The time step was 10 s for the outermost model and decreased to 2 s, 0.5 s for the finer models. Simulation starting time for the outermost (coarse) domain was set up on 17 June 2017 at 0600 UTC, while the simulation in the innermost domain (with the finest resolution) effectively starts at 1300 UTC. We performed multiple simulations to obtain the more realistic scenario of the atmospheric environment based on the CTI Report (2017) and Pinto et al. (2022). This preliminary study led to the decision to ignite the fires almost 1 h later. Indeed, this setting was in better agreement with what was actually observed. Basically, a gust front was observed reaching the Pedrógão region at 1700 UTC. Preliminary test simulations showed an analogous pattern, but approximately 1 h earlier when using ECMWF boundary conditions data.

The mesoscale environment simulated with 2 km spatial resolution showed the same features identified in previous studies. The dry thunderstorm environment documented by Couto et al. (2020) favoured the development of a mesoscale convective system during the afternoon which produced several outflows in Central Portugal (e.g., Pinto et al., 2022).

The next section focuses the results obtained on 80 m resolution, which are the most important for the description of the modelled pyroCb, and highlights the main findings for the Pedrógão Grande fire. These results are evaluated in view of what is described by Pinto et al. (2022), whose analysis is based directly on observations. The discussion will follow in Section 4.

3. Results

The present section provides a description of the fire environment observed in the 80 m resolution domain, which is the most important for the analysis of the main processes at the fire-scale.

Figure 3 shows the wind field at 100 m altitude and the evolution of the fire front at the surface, as described by the variable S. The first hours of the simulation were marked by a northerly wind-flow affecting the Pedrógão Grande region and a change in the wind direction after 1700 UTC (not shown). Fig. 3a shows Easterly and slightly South-easterly winds reaching the fire fronts at 1730 UTC with magnitudes between 6 and 8 m/s. From this moment on, the simulation shows a north-easterly (NE) wind-flow over the region, with slightly weaker intensities around 4 m/s (Fig. 3b). In the hour that follows an intensification of the wind flow is observed, with winds stronger than 8 m/s approaching the east of Pedrógão Grande (Fig. 3c). This NE flow hits the fire 15 min later at 1930 UTC (Fig. 3d).

As previously mentioned, the evolution of the fire front was forced by assigning an arrival time map based on actual reports. Not surprisingly this fire evolution is consistent with the local wind-field as observed in the simulation. The north winds favoured the displacement of the fire fronts southward during the first hours (see numbers 1 and 2 indicated in Fig. 3a), while changes in the wind field for *E*-NE induced the fire propagation in the west direction. This condition led to the junction of the two fire fronts in the region of Pedrógão Grande and the formation of a single merged fire front (see number 3 indicated in Fig. 3b-d).

Figure 4 shows the vertical structure of the smoke plume, as described by the condition $S \geq 0.01$ (we recall that S is a smoke tracer). At the beginning of the event, the smoke plumes in the Pedrógão Grande fires, i.e., associated with the ignition of "Escalos Fundeiros" and "Regadas", are transported southward in the lower troposphere (Fig. 4a). The smoke plume is transported to the Southwest direction an hour later and already reaches higher levels around 4 km altitude (Fig. 4b). Fig. 4c shows an intensification of the smoke plume, which extends up to the upper troposphere with a top exceeding 9 km altitude. At this instant, we observe the highest concentration of smoke westward of Pedrógão Grande fire. In addition, it is noteworthy that the smoke plume in Góis fire remains concentrated in the lower troposphere during the period (Fig. 4a-c).

The plume structure is illustrated further on Fig. 5 which displays a SW-NE vertical cross-section intersecting the fire front, represented by using values of turbulent kinetic energy well above 10 m^2/s^2 at surface. On the vertical sections we show contours of the smoke tracer (S) which highlights the plume structure between 1900 UTC and 1945 UTC. We observe a progressive intensification of the vertical extension of the plume which concentrates up to the middle levels until 1915 UTC (Fig. 5a-b) and reaches a maximum 10 km altitude at 1930 UTC (Fig. 5c). Fig. 5d indicates a possible disconnection of the smoke plume resulting from an interruption of vertical transport of smoke at 1945 UTC, with no smoke in the middle levels. On the other hand, the same figure presents smoke in the upper troposphere, which does not directly connect with the fire activity at the surface.

The vertical velocity field analysis reveals strong updraughts along the fire front. The smoke characteristics are illustrated in Fig. 5, while Fig. 6 superimpose three different instants of the vertical velocity field above 8 m/s. A convective column is observed to reach the mid troposphere at 1915 UTC (orange), which intensifies 15 min later and exceeds 8 km altitude (yellow). However, the upward motion created by the fire

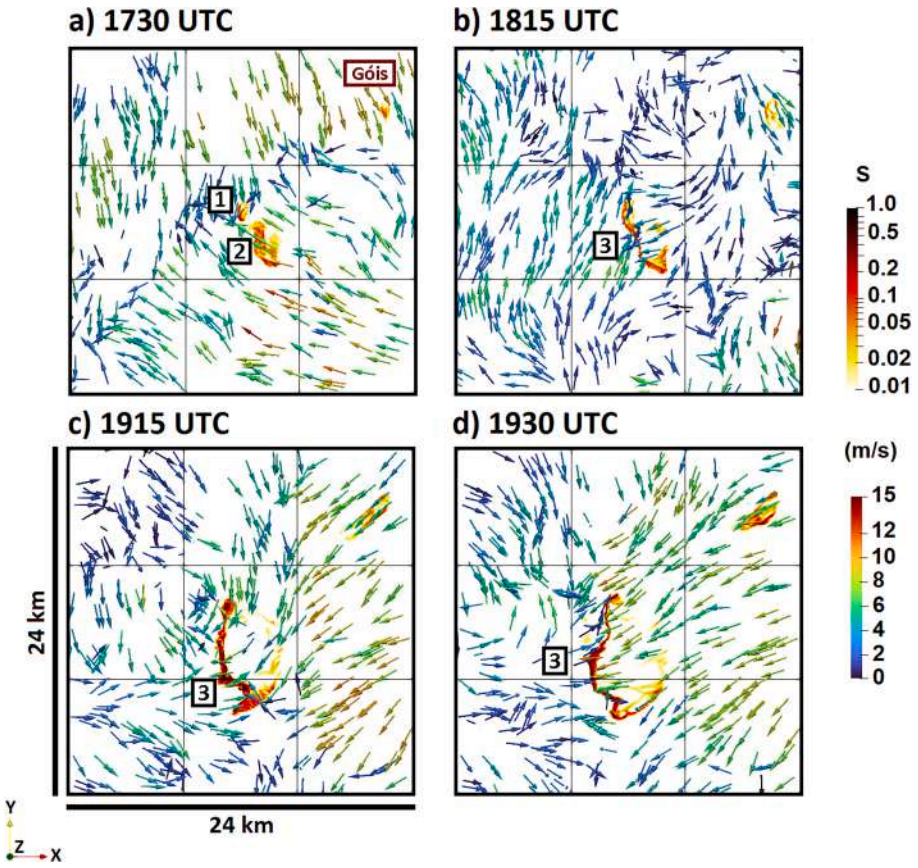

Fig. 3. The advancing fire front is illustrated through the relative smoke tracer concentration S at surface from the simulation at 80 m resolution (coloured areas). The arrows represent the horizontal wind magnitude at 100 m altitude on 17 June 2017 a) at 1730 UTC, b) at 1815 UTC, c) at 1915 UTC, and d) at 1930 UTC. The numbers 1 and 2 in Fig. 3a represent the fire fronts from the ignitions in "Regadas" and "Escalos Fundeiros", respectively. In turn, the number 3 in Figs. 3b-d represent the merged fire front.

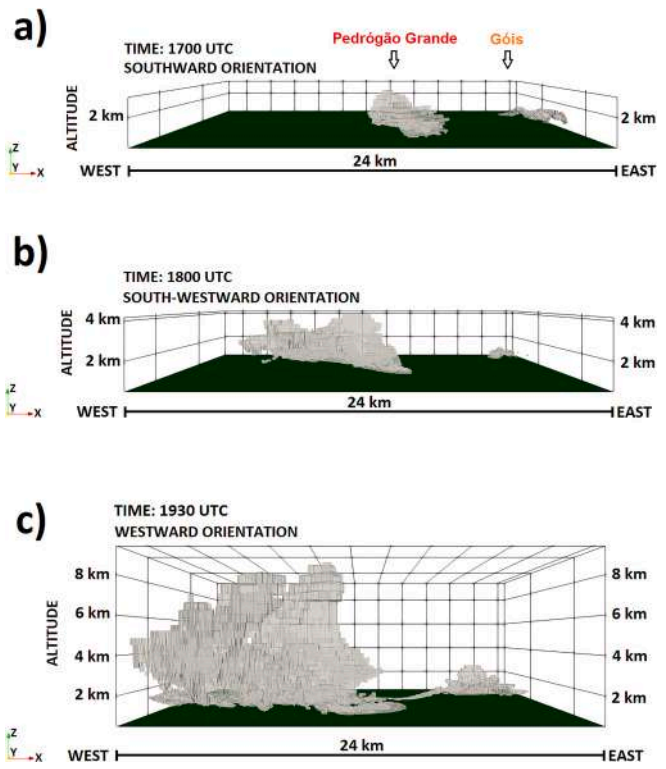

Fig. 4. 3D smoke plume structure represented by the relative smoke tracer concentration S from the simulation at 80 m resolution: a) at 1700 UTC, b) at 1800 UTC, and c) at 1930 UTC.

remains mostly below the middle levels at 1945 UTC (green), confirming the possible collapse of the convective column simulated at 1930 UTC.

Figure 7a displays a vertical cross-section through the convective column at 1930 UTC where upward motions with velocities around 25 m/s at 8 km altitude are shown. The response of the atmosphere to the emission of fluxes from the surface results in the production of turbulent flow in the fire environment, with turbulent kinetic energy (TKE) well above 10 m^2/s^2 throughout the convective column above the fire front at surface (Fig. 7b).

Figure 8 shows the mixing ratio of water vapour and total liquid and frozen water from a S—N oriented vertical cross-section intersecting the convective column at 1930 UTC. The total liquid water is computed as the sum of cloud droplets and rain drops mixing ratios. In the case of total frozen water, it was obtained from the sum of the mixing ratios of ice-crystals, snow-aggregate and graupel particles.

Figure 8a shows water vapour being vertically transported to the middle levels resulting in values >6 g/kg above 5 km altitude. The red contour represents values with total liquid water of 0.5 g/kg, whereas white contour the same amount of total frozen water. Fig. 8b represents the concentration of liquid water with maximums around 2.5 g/kg at 6 km altitude. At the same instant, a high concentration of frozen water is simulated with values around 4 and 5 g/kg between 8 km and 9 km altitude (Fig. 8c).

The regions of liquid and frozen water content of >0.5 g/kg are shown in Fig. 9. Fig. 9a shows a core of liquid water content extending to

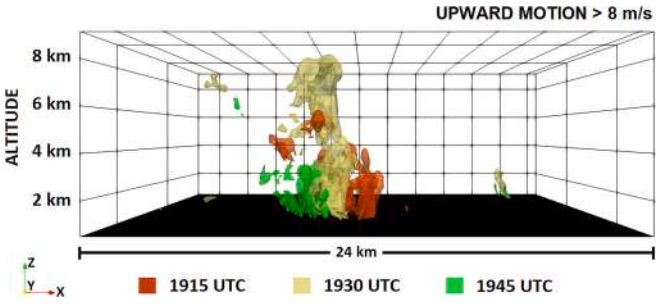

Fig. 6. 3D structure of the regions with upward motions above 8 m/s in three different instants of the pyroCb cloud development.

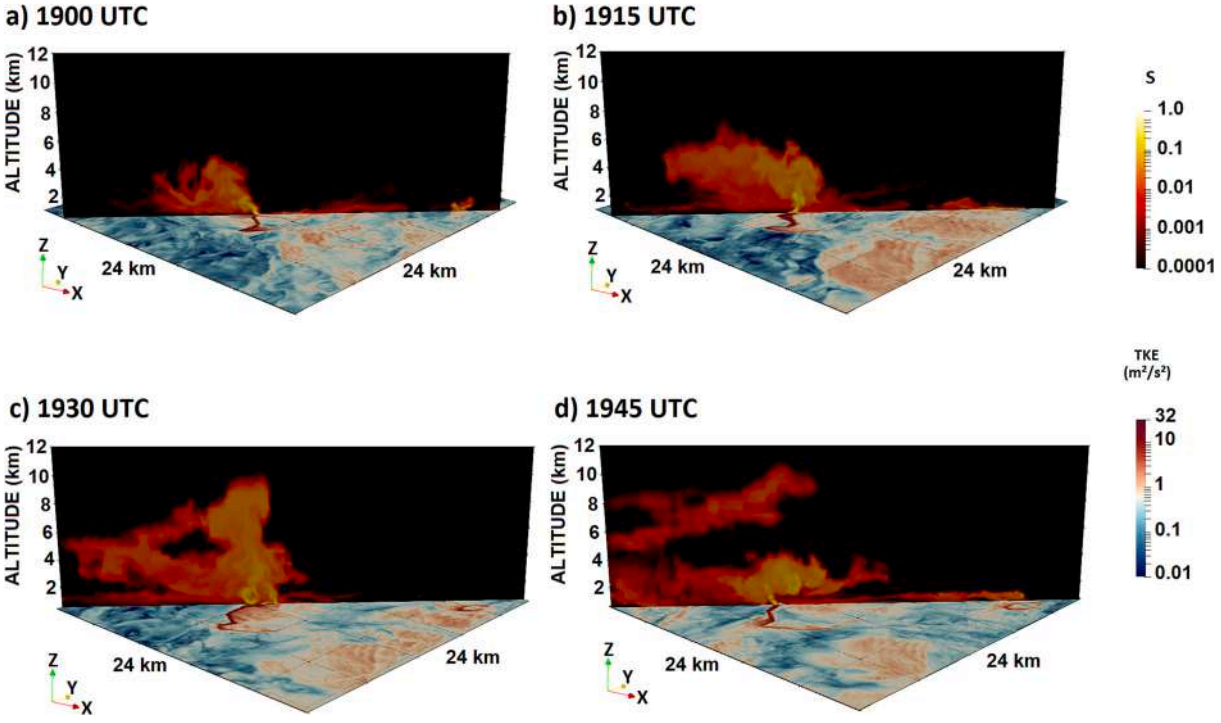

Fig. 5. SW-NE vertical cross-sections of the smoke tracer concentration S and turbulent kinetic energy (m^2/s^2) at surface a) at 1900 UTC, b) at 1915 UTC, c) at 1930 UTC, and d) at 1945 UTC.

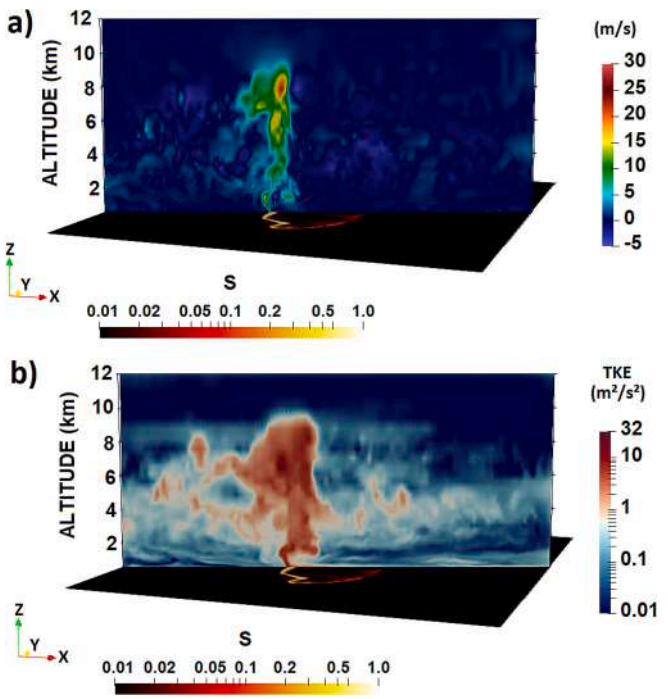

Fig. 7. Vertical cross section intersecting the plume at 1930 UTC: a) vertical velocity (m/s), and b) turbulent kinetic energy (m^2/s^2). The relative smoke tracer concentration S at surface represents the fire front location.

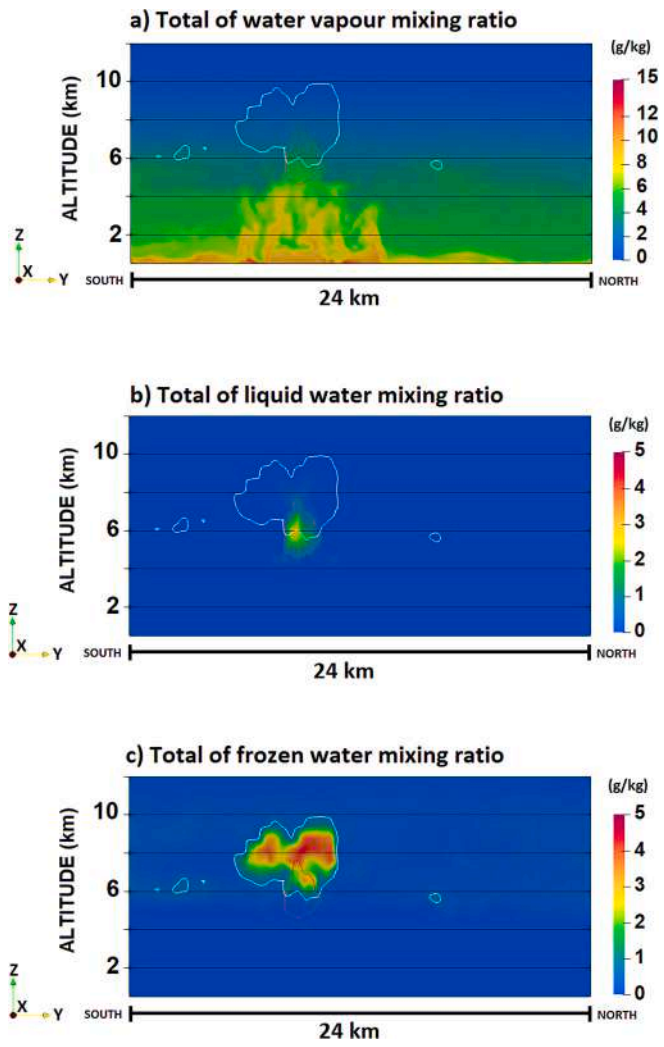

Fig. 8. S—N vertical cross section intersecting the plume at 1930 UTC: a) mixing ratio of water vapour, b) total liquid water mixing ratio (cloud droplets and rain drops), and c) total frozen water mixing ratio (graupel, snow-aggregate and ice crystals). The total liquid water content of 0.5 g/kg is represented by the red contour, whereas total frozen water content of 0.5 g/kg by white contour. (For interpretation of the references to colour in this figure legend, the reader is referred to the web version of this article.)

higher levels from the middle levels at 1930 UTC (orange). This core has been in a region of "inflow" when considering the pyro cloud system structure. The high concentration of liquid water is embedded in a large region of frozen water that extends westward. The figure also indicates that the smoke plume (see Fig. 4c) presented a significant concentration of hydrometeors in its upper portion. On the other hand, the model simulates, 15 min later, a region of liquid water to westward at lower levels, just above 2 km altitude (Fig. 9b). In this case, this core of liquid water is found in an "outflow" sector of the pyro cloud system. It is also worth noting the anvil of the mesoscale convective system that developed in the afternoon near the fire.

Figure 10 shows the vertical velocity field at 1945 UTC. Considering the 2.1 km altitude, Fig. 10a displays some regions of upward motions along the fire region with velocities above 10 m/s, and notoriously a region of intense downward motion with velocities larger than 10 m/s. Fig. 10b shows this downward motion extending from the middle levels toward the surface and maximum velocities around 15 m/s at 3 km altitude. Such a region coincides with the liquid water region identified in Fig. 9b. The outflow touches the surface around 2000 UTC, as can be seen in the turbulent kinetic energy field (Fig. 10c). It is important to note that this outflow developed from the fire-generated cloud system.

An additional point of interest is the time at which the smoke plume's upward movement ceased in the mid-levels of the atmosphere, with the goal of elucidating the short-lived nature of the convective column. Fig. 11a-b show the vertical velocity at middle levels (5 km altitude). The convective column is found at 1930 UTC (Fig. 11a) and no longer identified at 1945 UTC (Fig. 11b). The wind field analysis at the same level, but between 1915 UTC and 1945 UTC, indicates a southeasterly flow reaching the main convective column (Fig. 12a-c), whereas Fig. 12d shows a relative maximum of the horizontal wind magnitude at middle levels of around 11 m/s. The vertical profile presented in Fig. 12d is the extraction of the model values at the nearest grid point. This southeasterly flow may have counteracted the vertical movement, helping to interrupt the convective column.

In summary, the simulation exhibited the development of a deep convective cloud from the fire, which has been considered to be a pyroCb cloud in the present study. The fire-generated thunderstorm was simulated between 1915 UTC and 2000 UTC, with maximum development at 1930 UTC and the production of a very localized outflow touching the ground close to the 2000 UTC.

To complete the fire environment characterization, and after the identification of a pyroCb cloud development, Fig. 13 brings the vertical thermodynamic structure of the atmosphere in a point near the fire and at two different instants, namely 1500 UTC and 1900 UTC. Fig. 13a displays a hot and dry lower troposphere followed by a moist layer from the middle levels at 1500 UTC. The moment close to the beginning of the pyroCb development, at 1900 UTC, also shows a saturated middle troposphere and a drier layer below (Fig. 13b). Such an environment favours the development of pyro clouds if the smoke column is large enough to reach higher levels. In this case, the ascending motions associated with the smoke plume can be reinforced by the potential instability released in the middle troposphere by microphysical processes during cloud development.

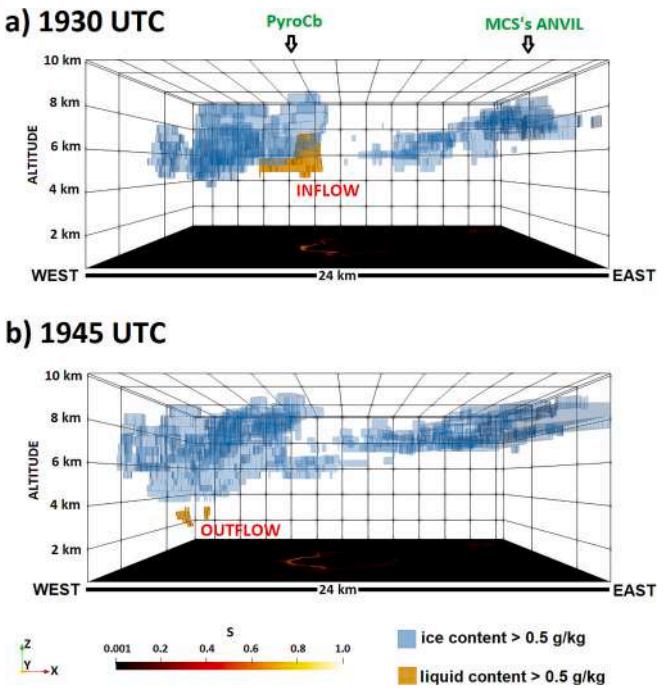

Fig. 9. 3D structure of the total liquid water content of 0.5 g/kg (orange) and total frozen water content of 0.5 g/kg (blue). The fire front is represented at surface from the relative smoke tracer concentration S: a) at 1930 UTC, and b) at 1945 UTC. (For interpretation of the references to colour in this figure legend, the reader is referred to the web version of this article.)

4. Discussion

The present study investigates the influence of an extreme wildfire event on the local atmospheric conditions using a fire-to-atmosphere numerical simulation. In 2017, the Portuguese territory was characterized by a particularly intense fire season. We present the results obtained using a numerical simulation of the deadliest event that occurred in that year.

The study focused on the main atmospheric phenomena induced by the simulated fire at a near fire scale. Some aspects are now discussed to compare with the observational study presented by Pinto et al. (2022) for the same wildfire episode. In general, the smoke plume remained in the lower atmosphere and was oriented southward during the first simulated hours. Regarding the vertical extension of the smoke plume, Pinto et al. (2022) presented an estimate of the smoke plume top on the basis of radar observations. They argued that during the first hours of the fire, the top of the plume was bounded below 4 km. This fact is consistent with the results obtained with the numerical model.

The model shows a low-level NE wind-flow approaching the fire from 1915 UTC. The occurrence of this flow played an important role in the intensification of the pyro-convective activity simulated at 1915 UTC. It reinforced the upward motions since a convective column extending vertically reached 10 km altitude with velocities around 20 m/s at 1930 UTC. Our simulated vertical velocities of 15–20 m/s are in agreement with previous observational studies, such as the velocities ranging from −15 to +30 m/s reported in intense pyroconvection events (Kingsmill et al., 2023). Over the following minutes, cloud development increased ahead westward and above the fire front, the cloud system maintained as a "stationary" thunderstorm anchored in the main convective column. Cunningham and Reeder (2009) showed the water production as a critical factor for a physically relevant simulation of such a cloud system. In our study, the convective column favoured both the rapid water vapour vertical transport to higher levels and the significant concentrations of liquid and frozen water, simulated within the convective column.

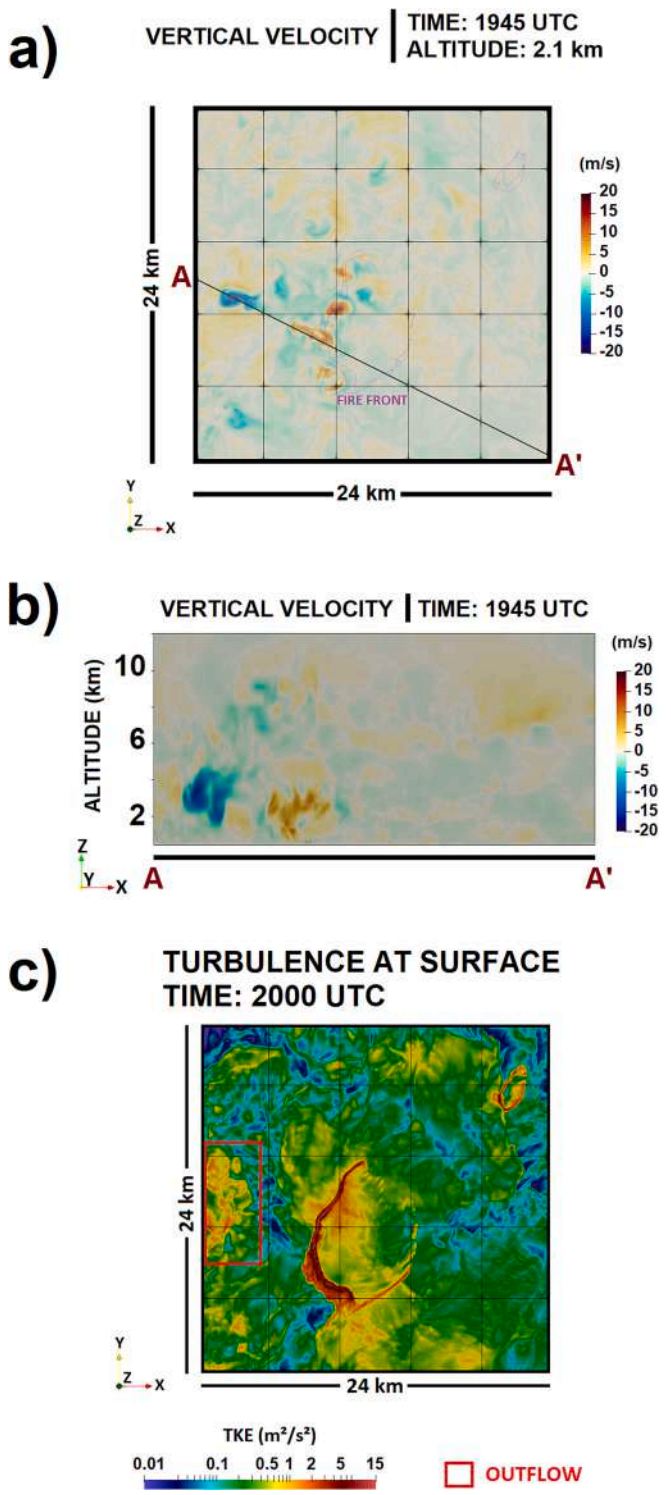

Fig. 10. a) Vertical velocity at 2.1 km altitude at 1945 UTC, b) A-A' vertical cross-section indicated in Fig. 10a with vertical velocity (m/s) at 1945 UTC, and c) turbulent kinetic energy (m^2/s^2) at surface at 2000 UTC. The purple contour in Fig. 10a represents the fire front. (For interpretation of the references to colour in this figure legend, the reader is referred to the web version of this article.)

Chang et al. (2015) argued that an increase in updraughts caused the production of rainwater content to grow. This fact provides an explanation to the high production of liquid water simulated in the main convective column from the middle levels. Moreover, the strong freeze, evident in the high concentration of ice particles, probably intensified

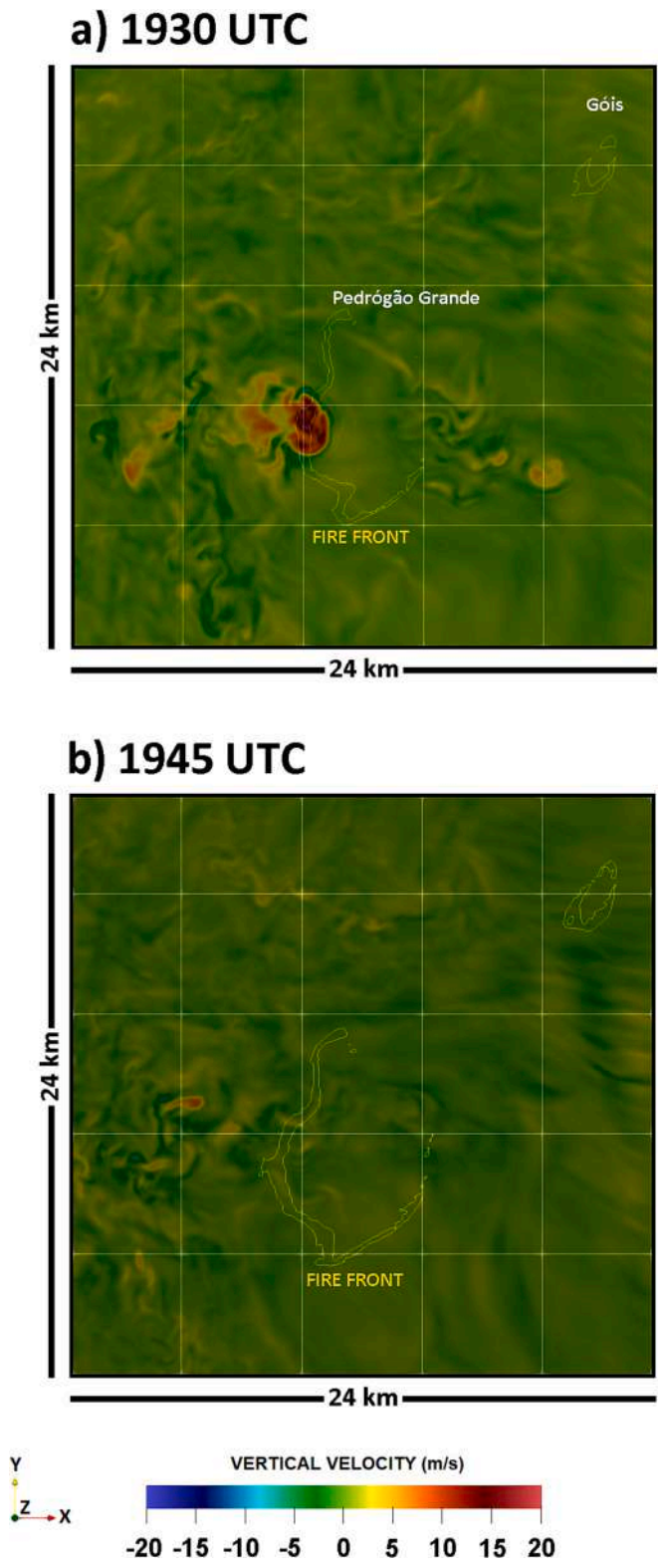

Fig. 11. Vertical velocity (m/s) at 5 km altitude a) at 1930 UTC, and b) 1945 UTC. The yellow contour represents the fire front. (For interpretation of the references to colour in this figure legend, the reader is referred to the web version of this article.)

the upward motions at 8 km altitude by releasing latent heat, and then favouring the convective column penetration into the upper troposphere. As mentioned in the introduction, under extreme wildfire conditions, intense convection is an efficient way to transport aerosols particles from the boundary layer to the upper troposphere or even in the lower stratosphere (e.g., Fromm and Servranckx, 2003; Peterson et al., 2018). Luderer et al. (2006), in turn, showed from numerical simulation that the atmospheric environment and the heat released from the fire are the key ingredients determining the evolution of a pyroCb cloud, as well as the intensity of the convection along the troposphere. These factors are also important to determine the impacts and lifetime of the pyroCb cloud system (e.g., Trentmann et al., 2006).

In the present case study, the simulation indicates that the strong convection over the plume weakened after 1930 UTC. A possible explanation for this is that the convective column that was extending throughout the troposphere suddenly stopped being sustained by the fire activity. Moreover, the model simulated the formation of downward vertical motions which organized as a very localized convective outflow westward ahead the Pedrógão Grande fire front. A southeasterly flow at middle levels could account for both the collapse of the convective column and the rapid formation of the pyroCb cloud. The cloud system lasted less than one hour and presented the mature stage within 15 min. It is noteworthy that Fromm et al. (2006) showed pyroCb clouds presenting a microscale diameter (10 km) but lasting a few hours (3 h).

Regarding the localized outflow that reached the surface just before 2000 UTC, the evaporation of the total liquid water content probably intensified the downward motions. This microscale phenomenon developed from the pyroCb cloud with vertical velocities of around 15 m/s at 3 km altitude. When compared to the Cumulonimbus cloud developing without interactions with fire and smoke, a strong suppression of precipitation is often observed in pyroCb clouds. This occurs since the presence of large concentrations of cloud condensation nuclei suppresses the formation of both wide water and ice hydrometeors (Rosenfeld et al., 2007). Luderer et al. (2006) also verified such feature using a cloud resolving model with a two-moment bulk microphysical scheme. Reutter et al. (2014) showed that the microphysical evolution of a pyroCb cloud system depends on the aerosol concentration. Unfortunately, the one-moment microphysical scheme used in this study does not allow to assess the impact of aerosol particles on the cloud microphysics. Moreover, we remark that the smoke tracer concentration (S) is a passive scalar whose purpose is only to visualize the evolution of the plume, and it does not interact with the hydrometeors (e.g., Baggio et al., 2022) and with the radiation.

Concerning the atmospheric environment in the fire scale, Couto et al. (2020) showed that Pedrógão Grande fire occurred under a dry thunderstorm's environment on the basis of the sounding from Lisbon, which is almost 200 km distant from Pedrógão Grande. The thermodynamic diagram obtained in the proximity of the fire was coherent with this previous study. The dry, hot, and windy conditions at the surface were observed below a moist layer at middle levels. This environment has been well known to favour the pyroCb activity during extremes wildfires (e.g., Peterson et al., 2017; Tory et al., 2018; Giannaros et al., 2022), and the simulation results support the hypothesis that the dry thunderstorm environment was a prerequisite for the development of a deep pyro cloud system over Pedrógão Grande fire. The sounding in Lisbon on 17 June 2017 at 1200 UTC (University of Wyoming, 2017), is characterized by a K index of 28.90 °C and a precipitable water of 29.17 mm. These are significant values when considering dry thunderstorms environment and are consistent with those presented by Senande-Rivera et al. (2022). The K index estimates the atmospheric stability based on the 850–500 hPa temperature lapse rate, moisture content at 850 hPa and the thickness of moist layer, and Senande-Rivera et al. (2022) reported that high values of precipitable water and K index (> 26 °C) are associated with environments where thunderstorms are likely to occur.

The simulation illustrates well the evolution of the Pedrógão Grande fire which shows an increasing complexity. The interaction of mesoscale circulation surrounding the fire played an important role in the intensification of the convective column. These changes in the fire environment and smoke plume structure were documented by Pinto et al. (2022), which showed the transition of the smoke plume to a convective

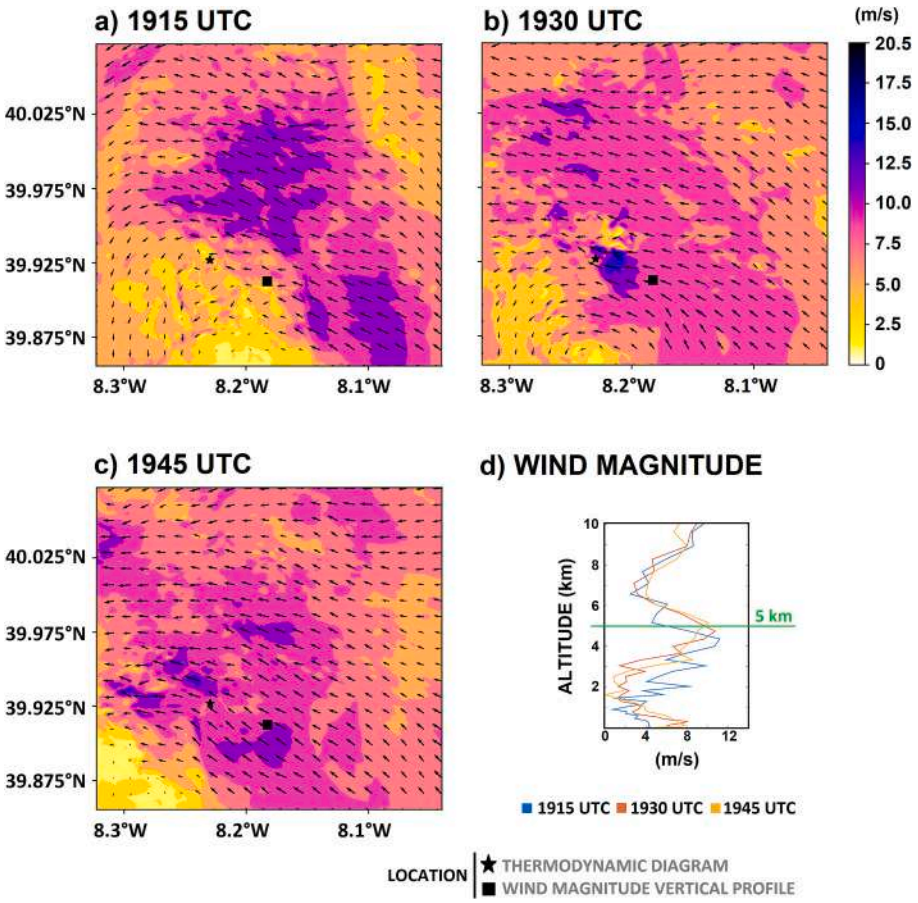

Fig. 12. Wind magnitude (coloured areas; m/s) and direction (arrows) at 5 km altitude a) at 1915 UTC, b) at 1930 UTC, and c) at 1945 UTC; d) Vertical profile of horizontal wind magnitude (m/s). The symbols in Fig. 12a – c indicate the location used to plot the thermodynamic diagram and the vertical profile of wind magnitude.

regime from 1830 UTC, as well as the changes in its orientation until 1910 UTC. In the simulation, the smoke plume is initially oriented south/south-westward to westward, leading to intense convection and the development of a pyroCb cloud. The approach of a low level NE wind-flow results in a sudden increase of the pyro-convective activity. Pinto et al. (2022) showed the smoke plume exceeding 12 km altitude at 1930 UTC (see Fig. 14 of Pinto et al., 2022). In the present study, the maximum smoke plume penetration height was simulated at around 10 km, but the time of occurrence is similar. We remark that it is not possible to confirm that the maximum smoke plume altitude observed corresponds to the convective column simulated at 1930 UTC. However, the simulation points to a good representation of some phenomena that may have occurred on the fire-scale during the Pedrógão Grande fire, when confronted with the main aspects documented in the reports and by Pinto et al. (2022).

The simulated pyroCb cloud did not present intense precipitation, but the fire activity created a strong convective column that transported smoke up to the upper troposphere and produced significant amount of liquid and frozen water inside the convective column at higher levels. Therefore, the intensification of the pyro-convective activity caused by the change in the surface wind direction was crucial for the explosive behavior and the ensuing cloud development. The transport of high amount of energy upward also occurred under favourable atmospheric conditions, namely an unstable middle troposphere.

5. Conclusions

The study presented the results obtained from a Meso-NH/ForeFire numerical simulation suitable for extreme fire conditions. For the case of study, the Pedrógão Grande megafire, the fire line evolution is described in detail by an official report. Considering this, the fire spatio-temporal propagation is assigned, rather than simulated, and the atmospheric behavior of the near-fire environment can be simulated with less incertitude.

The findings indicate that, with high spatio-temporal resolution, the model can effectively capture both the pyro-convective plume structure and the key processes in fire-atmosphere interactions. For instance, the notable change in the wind field caused by the interaction between the mesoscale environment and the fire contributed to changes in the smoke plume orientation well captured.

In the Pedrógão Grande fire event, the intense pyro-convective activity manifested as a pyroCumulonimbus cloud. The modelled pyroCb indicates that the complexity of the fire-atmosphere coupled system is well represented.

The pyroCb developed from the condensation inside the plume, where high concentrations of liquid and frozen water are observed. The convection was enhanced by the strong wildfire activity and latent heat released at higher levels, which penetrated the higher troposphere just above 10 km altitude. The strong updraughts created by the fire were crucial in establishing and maintaining the pyroCb by a few minutes. The main features of the simulated cloud system are in accordance with what reported by other studies of the same event (e.g., Pinto et al., 2022). However, such a cloud system lasted for a shorter time. We hypothesized that the approach of a southeast wind flow at middle levels led to the collapse of the main convective column, thereby interrupting the vertical transport of energy. In addition, extreme pyro-convective activity was also displayed in the simulation where we observe the development of an outflow originated from the pyroCb cloud. The

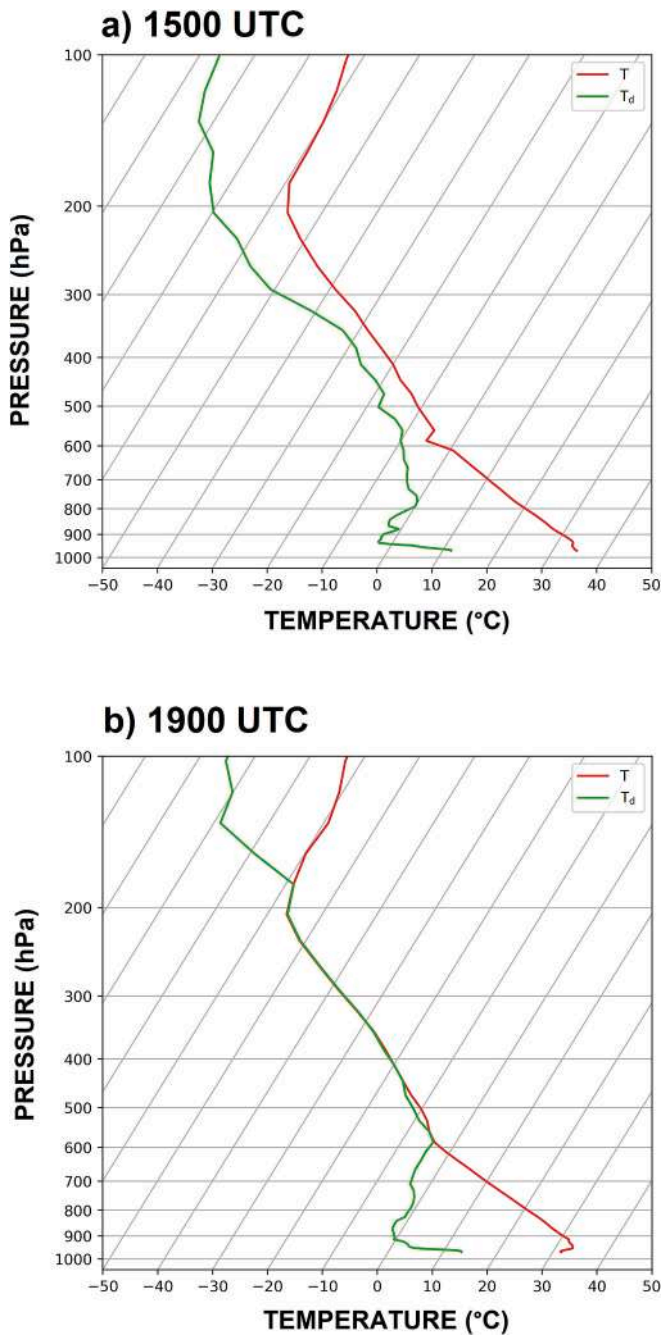

Fig. 13. Thermodynamic diagram simulated with 80 m horizontal resolution near Pedrógão Grande fire on 17 June 2017 a) at 1500 UTC, and b) at 1900 UTC.

evaporation of the liquid content caused an intensification of the downdraughts, which was simulated as a localized outflow ahead westward of the fire front of Pedrógão Grande fire.

This study provides important insights into the numerical modelling of fire-generated thunderstorms. We proved that the Meso-NH/ForeFire code can represent adequately the development of a fire-generated thunderstorm.

Aspects not covered in this study will be the focus of future research. These include the use of the Meso-NH/ForeFire code in the two-way mode, which will allow to study and evaluate the fire front evolution the local rate of spread, as well as investigate the coupled impact of a fire that would have started in different configuration and the associated potential predictability of the phenomenon using fully-coupled code in regards to this reference simulation. Finally, the use of a two-moment bulk microphysical scheme is advisable, since the physical phenomena related to the presence of fire aerosols are important aspects of pyroCb cloud systems and influence their impact on the atmosphere at all involved scales.

To conclude, this study demonstrates the significant contributions that numerical simulations, particularly using the Meso-NH/ForeFire code, can make to our understanding of severe wildfire events and pyro-convection. As a next step, we are now focusing on an analysis of fire behavior using a fully coupled model.

CRediT authorship contribution statement

Flavio Tiago Couto: Conceptualization, Methodology, Software, Visualization, Investigation, Formal analysis, Writing – original draft, Supervision, Project administration, Funding acquisition. **Jean-Baptiste Filippi:** Conceptualization, Methodology, Software, Resources, Supervision, Data curation, Writing – review & editing, Funding acquisition. **Roberta Baggio:** Software, Data curation, Writing – review & editing. **Cátia Campos:** Conceptualization, Data curation, Methodology, Software, Validation, Visualization, Formal analysis, Investigation, Writing – review & editing. **Rui Salgado:** Resources, Writing – review & editing, Project administration, Funding acquisition.

Declaration of competing interest

The authors declare that they have no known competing financial interests or personal relationships that could have appeared to influence the work reported in this paper.

Data availability

Data will be made available on request.

Acknowledgments

This research was funded by the national funds through FCT - Foundation for Science and Technology, I.P. under the PyroC.pt project (Refs. PCIF/MPG/0175/2019), ICT project (Refs. UIDB/04683/2020 and UIDP/04683/2020) and also by European Union through the European Regional Development Fund in the framework of the Interreg V A Spain - Portugal program (POCTEP) through the CILIFO project (Ref.: 0753-CILIFO-5-E), FIREPOCTEP project (0756-FIREPOCTEP-6-E), RH. VITA project (ALT20-05-3559-FSE-000074), H2020 FIRE-RES (GA: 101037419). The authors are grateful to the European Centre for Medium-Range Weather Forecasts (ECMWF) for the provided meteorological analysis and the supercomputing center of the University of Corsica under grant PIA UNITI ANR-22-EXES-0016 for their support on the coupled simulation computation.

References

Anderson, H.E., 1982. Aids to determining fuel models for estimating fire behavior. Gen. Tech. Rep. INT-122. U.S. Department of Agriculture, Forest Service, Intermountain Forest and Range Experiment Station, Ogden, Utah, p. 22.

Badlan, R.L., Sharples, J.J., Evans, J.P., McRae, R.H.D., 2021a. Factors influencing the development of violent pyroconvection. Part I: fire size and stability. Int. J. Wildland Fire 30 (7). https://doi.org/10.1071/WF20040.

Badlan, R.L., Sharples, J.J., Evans, J.P., McRae, R.H.D., 2021b. Factors influencing the development of violent pyroconvection. Part II: fire geometry and intensity. Int. J. Wildland Fire 30 (7). https://doi.org/10.1071/WF20041.

Baggio, R., Filippi, J.B., Truchot, B., Couto, F.T., 2022. Local to continental scale coupled fire-atmosphere simulation of large industrial fire plume. Fire Saf. J. 103699 https://doi.org/10.1016/j.firesaf.2022.103699.

Campos, C., Couto, F.T., Filippi, J.-B., Baggio, R., Salgado, R., 2023. Modelling pyro-convection phenomenon during a mega-fire event in Portugal. Atmos. Res. 290, 106776 https://doi.org/10.1016/j.atmosres.2023.106776.

Champeaux, J.-L., Han, K.-S., Geiger, B., Masson, V., 2005. Ecoclimap 2: a new approach at global scale for ecosystems mapping and associated surface parameters database

using SPOT/VEGETATION data. In: ECMWF/ELDAS Workshop on Land Surface Assimilation, 8-11 November 2004.
Chang, D., Cheng, Y., Reutter, P., Trentmann, J., Burrows, S.M., Spichtinger, P., Nordmann, S., Andreae, M.O., Pöschl, U., Su, H., 2015. Comprehensive mapping and characteristic regimes of aerosol effects on the formation and evolution of pyro-convective clouds. Atmos. Chem. Phys. 15, 10325–10348. https://doi.org/10.5194/acp-15-10325-2015.
Cheremisin, A.A., Marichev, V.N., Bochkovskii, D.A., et al., 2022. Stratospheric Aero-sol of Siberian Forest fires according to Lidar Observations in Tomsk in August 2019. Atmos. Ocean Opt. 35, 57–64. https://doi.org/10.1134/S1024856022010043.
Couto, F.T., Iakunin, M., Salgado, R., Pinto, P., Viegas, T., Pinty, J.-P., 2020. Light-ning modelling for the research of forest fire ignition in Portugal. Atmos. Res. 242, 104993 https://doi.org/10.1016/j.atmosres.2020.104993.
Couto, F.T., Santos, L.M.S., Campos, C., Andrade, N., Purificação, C., Salgado, R., 2022. Is Portugal starting to Burn all Year Long? The Transboundary Fire in January 2022. Atmosphere 13 (10). https://doi.org/10.3390/atmos13101677.
Cunningham, P., Reeder, M.J., 2009. Severe convective storms initiated by intense wildfires: Numerical simulations of pyro-convection and pyro-tornadogenesis. Geophys. Res. Lett. 36, L12812. https://doi.org/10.1029/2009GL039262.
Cuxart, J., Bougeault, P., Redelsperger, J.-L., 2000. A turbulence scheme allowing for meso-scale and large-eddy simulations. Q. J. R. Meteorol. Soc. 126, 1–30. https://doi.org/10.1002/qj.49712656202.
Dowdy, A.J., Ye, H., Pepler, A., et al., 2019. Future changes in extreme weather and pyroconvection risk factors for Australian wildfires. Sci. Rep. 9, 10073. https://doi.org/10.1038/s41598-019-46362-x.
Filippi, J.-B., Bosseur, F., Mari, C., Lac, C., Le Moigne, P., Cuenot, B., Veynante, D., Cariolle, D., Balbi, J.-H., 2009. Coupled atmosphere–wildland fire modelling. J. Adv. Model. Earth Syst. 2 https://doi.org/10.3894/JAMES.2009.1.11.
Filippi, J.-B., Bosseur, F., Pialat, X., Santoni, P.-A., Strada, S., Mari, C., 2011. Simulation of coupled Fire/Atmosphere Interaction with the MesoNH-ForeFire Models. J. Comb. Des. 2011, 1–13. https://doi.org/10.1155/2011/540390.
Filippi, J.-B., Bosseur, F., Mari, C., Lac, C., 2018. Simulation of a large Wildfire in a coupled Fire-Atmosphere Model. Atmosphere. 9 (6), 218. https://doi.org/10.3390/atmos9060218.
Fromm, M., Tupper, A., Rosenfeld, D., Servranckx, R., McRae, R., 2006. Violent pyro-convective storm devastates Australia's capital and pollutes the stratosphere. Geophys. Res. Lett. 33, L05815. https://doi.org/10.1029/2005GL025161.
Fromm, M., Lindsey, D.T., Servranckx, R., Yue, G., Trickl, T., Sica, R., Doucet, P., Godin-Beekmann, S., 2010. The Untold Story of Pyrocumulonimbus. Bull. Am. Meteorol. Soc. 91 (9), 1193–1210. https://doi.org/10.1175/2010BAMS3004.1.
Fromm, M.D., Servranckx, R., 2003. Transport of forest fire smoke above the tropo-pause by supercell convection. Geophys. Res. Lett. 30, 1542. https://doi.org/10.1029/2002GL016820.
Fromm, M.D., Kablick, G.P., Peterson, D.A., Kahn, R.A., Flower, V.J.B., Seftor, C.J., 2021. Quantifying the source term and uniqueness of the August 12, 2017 Pacific Northwest pyroCb event. J. Geophys. Res. Atmos. 126 https://doi.org/10.1029/2021JD034928 e2021JD034928.
Gerasimov, V.V., Zuev, V.V., Savelieva, E.S., 2019. Traces of Canadian pyrocumulo-nimbus clouds in the stratosphere over Tomsk in June-July, 1991. Atmos. Ocean Opt. 32, 316–323. https://doi.org/10.1134/S1024856019030096.
Giannaros, T.M., Papavasileiou, G., Lagouvardos, K., Kotroni, V., Dafis, S., Karagi-annidis, A., Dragozi, E., 2022. Meteorological analysis of the 2021 extreme wild-fires in greece: lessons learned and implications for early warning of the potential for pyroconvection. Atmosphere. 13 (3), 475. https://doi.org/10.3390/atmos13030475.
Guerreiro, J., Fonseca, C., Salgueiro, A., Fernandes, P., Lopez Iglésias, E., de Neufville, R., Mateus, F., Castellnou Ribau, M., Sande Silva, J., Moura, J.M., et al., 2018. Avalia-ção dos Incêndios Ocorridos Entre 14 e 16 de Outubro de 2017 em Portugal Continen-tal. In: Relatório Final; CTI Report 2018. Comissão Técnica Independente (CTI), Assem-Bleia da República, Lisboa, Portugal, p. 274.
Khaykin, S., Legras, B., Bucci, S., et al., 2020. The 2019/20 Australian wildfires gener-ated a persistent smoke-charged vortex rising up to 35 km altitude. Commun. Earth Environ. 1, 22. https://doi.org/10.1038/s43247-020-00022-5.
Kingsmill, D.E., French, J.R., Lareau, N.P., 2023. In situ microphysics observations of intense pyroconvection from a large wildfire. Atmos. Chem. Phys. 23, 1–21. https://doi.org/10.5194/acp-23-1-2023.
Lac, C., Chaboureau, J.-P., Masson, V., Pinty, J.-P., Tulet, P., Escobar, J., Leriche, M., Barthe, C., Aouizerats, B., Augros, C., Aumond, P., Auguste, F., Bechtold, P., Berthet, S., Bielli, S., Bosseur, F., Caumont, O., Cohard, J.-M., Colin, J., Couvreux, F., 2018. Overview of the Meso-NH model version 5.4 and its applications. Geosci. Model Dev. 11 (5), 1929–1969. https://doi.org/10.5194/gmd-11-1929-2018.
Lang, T.J., Rutledge, S.A., Dolan, B., Krehbiel, P., Rison, W., Lindsey, D.T., 2014. Lightning in Wildfire Smoke Plumes Observed in Colorado during Summer 2012. Mon. Weather Rev. 142 (2), 489–507. https://doi.org/10.1175/mwr-d-13-00184.1.
Lareau, N.P., Nauslar, N.J., Abatzoglou, J.T., 2018. The Carr fire vortex: a case of pyrotornadogenesis? Geophys. Res. Lett. 45, 13,107–13,115. https://doi.org/10.1029/2018GL080667.
Lareau, N.P., Nauslar, N.J., Bentley, E., Roberts, M., Emmerson, S., Brong, B., Mehle, M., Wallman, J., 2022. Fire-Generated Tornadic Vortices. Bull. Am. Meteorol. Soc. 103 (5), E1296–E1320. https://doi.org/10.1175/BAMS-D-21-0199.1.
Linley, G.D., Jolly, C.J., Doherty, T.S., Geary, W.L., Armenteras, D., Belcher, C.M., Bliege Bird, R., Duane, A., Fletcher, M.-S., Giorgis, M.A., Haslem, A., Jones, G.M., Kelly, L. T., Lee, C.K.F., Nolan, R.H., Parr, C.L., Pausas, J.G., Price, J.N., Regos, A., Nimmo, D. G., 2022. What do you mean, 'megafire'? Glob. Ecol. Biogeogr. 31, 1906–1922. https://doi.org/10.1111/geb.13499.
Luderer, G., Trentmann, J., Winterrath, T., Textor, C., Herzog, M., Graf, H.F., An-dreae, M.O., 2006. Modeling of biomass smoke injection into the lower stratosphere by a large forest fire (Part II): sensitivity studies. Atmos. Chem. Phys. 6, 5261–5277. https://doi.org/10.5194/acp-6-5261-2006.
Masson, V., Le Moigne, P., Martin, E., Faroux, S., Alias, A., Alkama, R., Belamari, S., Barbu, A., Boone, A., Bouyssel, F., Brousseau, P., Brun, E., Calvet, J.-C., Carrer, D., Decharme, B., Delire, C., Donier, S., Essaouini, K., Gibelin, A.-L., Giordani, H., Ha-bets, F., Jidane, M., Kerdraon, G., Kourzeneva, E., Lafaysse, M., Lafont, S., Lebeaupin Brossier, C., Lemonsu, A., Mahfouf, J.-F., Marguinaud, P., Mokhtari, M., Morin, S., Pigeon, G., Salgado, R., Seity, Y., Taillefer, F., Tanguy, G., Tulet, P., Vincendon, B., Vionnet, V., Voldoire, A., 2013. The SURFEXv7.2 land and ocean surface platform for coupled or offline simulation of earth surface variables and fluxes. Geosci. Model Dev. 6, 929–960. https://doi.org/10.5194/gmd-6-929-2013.
McCarthy, N., Guyot, A., Dowdy, A., McGowan, H., 2019. Wildfire and weather radar: a review. J. Geohys. Res. D. 124, 266–286. https://doi.org/10.1029/2018JD029285.
McRae, R.H.D., Sharples, J.J., Fromm, M., 2015. Linking local wildfire dynamics to pyroCb development. Nat. Hazards Earth Syst. Sci. 15, 417–428. https://doi.org/10.5194/nhess-15-417-2015.
Mlawer, E.J., Taubman, S.J., Brown, P.D., Iacono, M.J., Clough, S.A., 1997. Radiative transfer for inhomogeneous atmospheres: RRTM, a validated correlated-k model for the longwave. J. Geophys. Res. 102 (D14), 16 663–16 682. https://doi.org/10.1029/97JD00237.
Peterson, D.A., Hyer, E.J., Campbell, J.R., Solbrig, J.E., Fromm, M.D., 2017. A Conceptual Model for Development of intense Pyrocumulonimbus in Western North America. Mon. Weather Rev. 145 (6), 2235–2255. https://doi.org/10.1175/MWR-D-16-0232.1.
Peterson, D.A., Campbell, J.R., Hyer, E.J., et al., 2018. Wildfire-driven thunderstorms cause a volcano-like stratospheric injection of smoke. npj. Clim. Atmos. Sci. 1, 30. https://doi.org/10.1038/s41612-018-0039-3.
Peterson, D.A., Fromm, M.D., McRae, R.H.D., et al., 2021. Australia's Black Summer pyrocumulonimbus super outbreak reveals potential for increasingly extreme stratospher-ic smoke events. npj. Clim. Atmos. Sci. 4, 38. https://doi.org/10.1038/s41612-021-00192-9.
Pinto, P., Silva, Á.P., Viegas, D.X., Almeida, M., Raposo, J., Ribeiro, L.M., 2022. Influence of convectively driven flows in the course of a large fire in Portugal: the Case of Pedrógão Grande. Atmosphere 2022 (13), 414. https://doi.org/10.3390/atmos13030414.
Pinty, J.-P., Jabouille, P., 1998. A mixed-phase cloud parameterization for use in a mesoscale non-hydrostatic model: Simulations of a squall line and of orographic precipi-tation. In: Bull. Am. Meteorol. Soc. Proc. Conf. of Cloud Physics, Everett, WA, USA.
Ranjbar, K., O'Neill, N.T., Lutsch, E., McCullough, E.M., AboEl-Fetouh, Y., Xian, P., Strong, K., Fioletov, V.E., Sesins, G., Abboud, I., 2019. Extreme smoke event over the high Arctic. Atmos. Environ. 218, 117002 https://doi.org/10.1016/j.atmosenv.2019.117002.
Report, C.T.I., 2017. 2017. In: Análise e Apuramento dos Factos Relativos Aos Incêndios Que Ocorreram Em Pedrógão Grande, Castanheira de Pera, Ansião, Alvaiázere, Figueiró dos Vinhos, Arganil, Góis, Penela, Pampilhosa da Serra, Oleiros e Sertã, Entre 17 e 24 de Junho de 2017. Comissão Técnica Independente (CTI), Assembleia da República, Lis-boa, Portugal, p. 296.
Reutter, P., Trentmann, J., Seifert, A., Neis, P., Su, H., Chang, D., Herzog, M., Wernli, H., Andreae, M.O., Pöschl, U., 2014. 3-D model simulations of dynamical and mi-crophysical interactions in pyroconvective clouds under idealized conditions. Atmos. Chem. Phys. 14, 7573–7583. https://doi.org/10.5194/acp-14-7573-2014.
Rosenfeld, D., Fromm, M., Trentmann, J., Luderer, G., Andreae, M.O., Servranckx, R., 2007. The Chisholm firestorm: observed microstructure, precipitation and lightning activity of a pyro-cumulonimbus. Atmos. Chem. Phys. 7, 645–659. https://doi.org/10.5194/acp-7-645-2007.
Senande-Rivera, M., Insua-Costa, D., Miguez-Macho, G., 2022. Towards an atmosphere more favourable to firestorm development in Europe. Environ. Res. Lett. 17 (9), 1748–9326, 094015. https://doi.org/10.1088/1748-9326/ac85ce.
Sharples and Hilton, 2020. Modeling vorticity-driven wildfire behavior using near-field techniques. Front. Mech. Eng. 5, 69. https://doi.org/10.3389/fmech.2019.00069.
Tarshish, N., Romps, D.M., 2022. Latent heating is required for firestorm plumes to reach the stratosphere. J. Geophys. Res. Atmos. 127 https://doi.org/10.1029/2022JD036667.
Tory, K.J., Thurston, W., Kepert, J.D., 2018. Thermodynamics of Pyrocumulus: a Conceptual Study. Mon. Weather Rev. 146 (8), 2579–2598. https://doi.org/10.1175/MWR-D-17-0377.1.
Trentmann, J., Luderer, G., Winterrath, T., Fromm, M.D., Servranckx, R., Textor, C., Herzog, M., Graf, H.-F., Andreae, M.O., 2006. Modeling of biomass smoke injection into the lower stratosphere by a large forest fire (part I): reference simulation. Atmos. Chem. Phys. 6, 5247–5260. https://doi.org/10.5194/acp-6-5247-2006.
University of Wyoming, 2017. Available online at: https://weather.uwyo.edu/upperair/sounding.html (last access on 03 March 2023).
Verrelle, A., Ricard, D., Lac, C., 2015. Sensitivity of high-resolution idealized simulations of thunderstorms to horizontal resolution and turbulence parametrization. Q.J.R. Meteorol. Soc. 141, 433–448. https://doi.org/10.1002/qj.2363.